Free-Flight Trajectory Simulation of the ADEPT Sounding Rocket Test Using CFD

Jakob D. Hergert[*]

Stanford University, Stanford, CA, 94305

Joseph M. Brock[†]

AMA, Inc., Moffett Field, CA, 94035

Eric C. Stern[‡], Michael C. Wilder[§]

NASA Ames Research Center, Moffett Field, CA, 94035

and David W. Bogdanoff[¶]

AMA, Inc., Moffett Field, CA, 94035

A computational study of the Adaptive Deployable Entry and Placement Technology (ADEPT) Sounding Rocket (SR-1) Test is presented using the US3D flow solver. ADEPT SR-1 is intended, in part, to assess the dynamic stability of this entry vehicle architecture. Given that no dynamic stability data exists for the ADEPT geometry, a limited ballistic range campaign has been performed to characterize the vehicle's stability characteristics pre-flight for Mach numbers between 1.21 and 2.5. Here, this data is used to assess the accuracy of US3D's free-flight CFD capability. Computed trajectories from US3D and experimental data show that the flow solver compares well in vehicle oscillation frequency, downrange distance, and oscillatory amplitude during high Mach number flight ($M_{avg} = 2.36$). For Mach numbers below 1.5, the solver under predicts total angle-of-attack by an average of $\sim 16\%$, but compares well in oscillatory frequency and downrange distance. Additionally, a capability for simulating the trajectory of the flight article through the atmosphere using CFD is presented. This capability couples US3D's free-flight capability to an atmosphere model that accounts for changes in free-stream density and temperature as the vehicle descends. Two simulations for the purpose of demonstrating the capability and viability of this approach are applied to SR-1 flight article, and some unique challenges are discussed.

Nomenclature

A	Area of Vehicle or Model
a	Speed of Sound
C_D	Drag Coefficient
m	Mass
M	Mach Number
α	Angle of Attack
ψ	Yaw Angle
ρ	Density
μ	Fluid Viscosity

---

[*]Graduate Student, jhergert@stanford.edu, AIAA Student Member

[†]Aerothermodynamicist, Aerothermodynamics Branch, AIAA Member

[‡]Research Engineer, Thermal Protection Systems Branch, AIAA Member

[§]Aerospace Engineer, Aerothermodynamics Branch, AIAA Associate Fellow

[¶]Senior Research Scientist, AMA, Inc., AIAA Associate Fellow

American Institute of Aeronautics and Astronautics

I. Introduction

ENTRY, Descent, and Landing (EDL) is a crucial part to the success of any planetary entry mission. During the descent phase, the vehicle decelerates from hypervelocity entry speeds down to mid- to low-supersonic speeds. During this deceleration, vehicle stability and attitude are accounted for by passive means such as geometry design and center of gravity offset, or active means through the use of a Reaction Control System (RCS). The amount of control that is needed depends on the stability of the free-flight behavior of the vehicle, characterized as stable or unstable, and is determined by its aerodynamic coefficients. Currently, these coefficients are obtained through a combination of wind-tunnel, ballistic range, and flight test experimentation.

Legacy planetary probe designs have the advantage of a long history of testing and flight dynamic characterization. However, in response to increased interest in human-rated missions to Mars that require landing masses which exceed current legacy systems, NASA is developing several new EDL systems that have the potential to meet the increased demands of human payloads. One such technology is the Adaptive Deployable Entry and Placement Technology (ADEPT).[1] The downside of a novel design such as ADEPT is the limited experimental flight data pertaining to the vehicle's dynamics. NASA has recently commissioned a sounding rocket test (SR-1) of a scaled down geometry (Nano-ADEPT)[2] in order to acquire an initial assessment of the vehicle's free-flight behavior. The Nano-ADEPT geometry can be seen in Figure 1. Blunt bodies, such as Nano-ADEPT, have been shown to have favorable heating characteristics during hypersonic descent, but inherently unstable behavior while traveling at low supersonic Mach numbers.[3,4] To further characterize the dynamics of Nano-ADEPT in the low-supersonic regime pre-flight, a ballistic-range study has been completed.

While experimental methods such as the ballistic range are considered the gold standard in obtaining aerodynamic coefficients, it can be prohibitively expensive to perform a full suite of experiments for each design iteration. Additionally, full flight similitude may be difficult to achieve. Computational Fluid Dynamic (CFD) simulations currently offer a relatively inexpensive way to assess static stability. A database can be obtained using CFD containing hundreds of simulations across a wide variation of flight parameters requiring only a few discrete points be anchored by experimental data. And yet, it is desirable to have a similar capability for assessing free-flight aerodynamic stability using CFD.

The scope of this paper is to develop, characterize, and verify methodologies to simulate free-flight behavior using ADEPT SR-1 as a test case. The SR-1 flight article is expected to see a rapid change in atmospheric density throughout its trajectory. As a result, we desire to implement a routine that can simulate the full flight-relevant trajectory with changing atmospheric conditions. To this end, this work will be divided into two sections. In order to assess the validity of CFD simulations as they apply to trajectories, the first section aims to extend previous efforts by Brock *et al.*[5] and Stern *et al.*[6,7] by continuing the validation and development of the free-flight capability within the CFD tool US3D.[8] This will be achieved through several simulations of, and comparison to, the ADEPT SR-1 ballistic range experiments. The second portion of the paper will present a novel method for free-flight, 6 degree of freedom (DOF) trajectory simulations using US3D. This method aims to move beyond the constraints imposed in traditional CFD simulations by offering the capability to fly through changing atmospheric conditions. Consequently, insight will be gained regarding the feasibility and potential pitfalls of doing full-scale free-flight trajectory simulations.

II. ADEPT SR-1

The ADEPT project is one of several systems under development at NASA that have the potential to land larger payloads on Mars.[1] In order to rapidly develop the technology, ADEPT has been re-sized and re-purposed as a platform to land small secondary payloads such as cubesats in locations of interest.[9] The fully deployed configuration can be seen in Figure 1. Nano-ADEPT uses a system of mechanical ribs and flexible carbon cloth as its primary heat shield and structure. During launch, this system is stowed to save volume in the payload shroud of the rocket. After jettison from the launch or transfer vehicle, it is deployed using a system of mechanical springs in an umbrella-like fashion prior to its descent into the atmosphere. When fully deployed, Nano-ADEPT is a cone with a 70° cone angle, a diameter of 0.70 meters, and a length of 0.32 meters.

American Institute of Aeronautics and Astronautics

The Nano-ADEPT geometry has several distinguishing features that could affect the capsule's aerodynamics when compared to previous capsule designs. Instead of a traditional backshell, the aft-body of Nano-ADEPT is open with a large protruding payload down the axis of symmetry. Additionally, the mechanical rib-cloth system results in a forebody consisting of faceted panels instead of a fully axisymmetric sphere-cone. Furthermore, all sections of the forebody panels interface with a rigid nose cap that is not completely flush with the surface of the main heat shield. This introduces a backward facing step into the forebody flow-field that could cause flow separation. Configurations such as this are rarely implemented as EDL geometries and their effects on stability are seldom studied or understood.

An illustration of the ADEPT SR-1 mission can be seen in Figure 1. SR-1 will be launched from Spaceport America, New Mexico on a Spaceloft XL rocket manufactured by Up Aerospace. Nano-ADEPT will be ejected from the payload shroud after the rocket conducts a maneuver to reduce the spin rate. Following ejection, the capsule will deploy its carbon fabric skirt prior to reaching apogee and then re-accelerate into Earth's atmosphere to a peak Mach number of at least $M = 3$ at a near-vertical flight-path angle. Because of the near-vertical flight-path angle, Nano-ADEPT is expected to see a rapid and substantial variation in atmospheric conditions throughout descent. The EDL portion of the flight test consists of deceleration from Mach 3 to Mach 1 through altitudes between 60-70 km and 30 km. After deceleration, ADEPT will land in White Sands, New Mexico where the instrumentation will be recovered. The flight test hopes to validate the operation of Nano-ADEPT's deployment architecture as well as its re-entry stability and dynamics.[10]
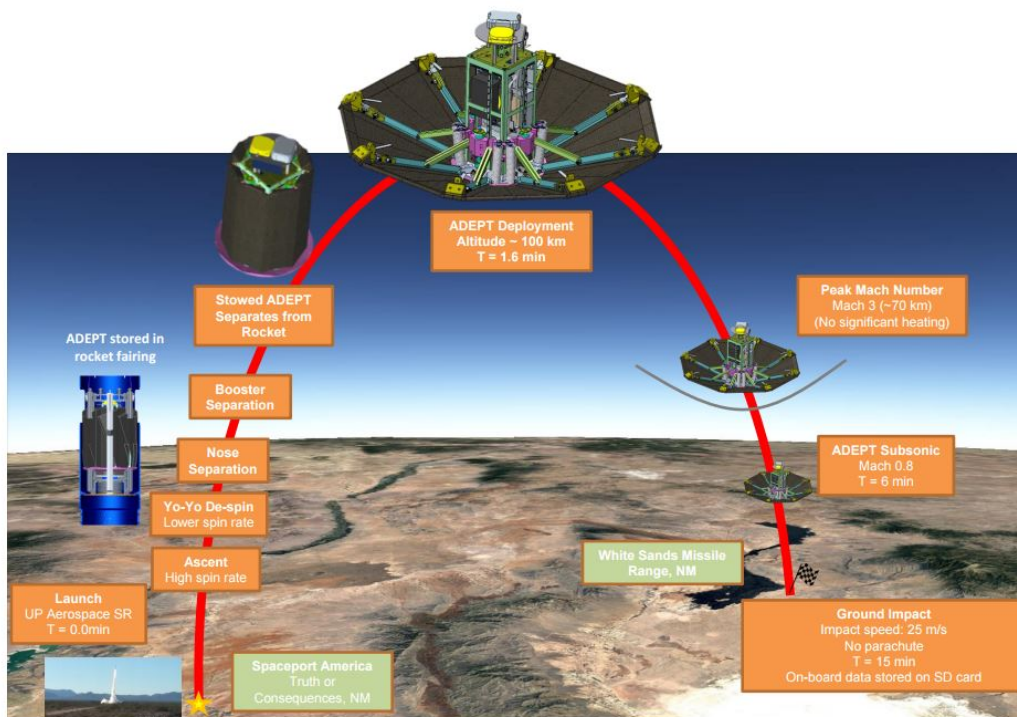

Figure 1: Concept of Operations: ADEPT SR-1.[10]

III. ADEPT SR-1 Ballistic Range Test and Simulation

The ultimate goal of SR-1 is to show stability through the full atmospheric descent, but the "threshold" performance parameter for ADEPT SR-1 is stable flight through Mach numbers down to $M = 1.8$. Given that no dynamic stability data exists for faceted blunt body geometries of 70° forebody half-angle, there was a concern that the vehicle could tumble as it decelerates through supersonic speeds. A ballistic range test was undertaken to examine the dynamic stability characteristics of the Nano-ADEPT configuration pre-flight. The test was limited in scope, targeting the stability characteristics at Mach numbers from $M = 1.2$ to $M = 2.5$, and not intended to develop an aerodynamic database.

American Institute of Aeronautics and Astronautics

A. Test Facility and Model Properties

The tests were conducted in the Hypervelocity Free-Flight Aerodynamics Facility (HFFAF)[11] at NASA Ames Research Center. Using one of a suite of available guns, the facility offers the capability of testing over the full speed range experienced by entry vehicles, from hypersonic to subsonic. In addition, the test gas pressure can be varied to allow independent control of the Mach and Reynolds numbers, and the gas composition can be selected to allow simulation of flight through different planetary atmospheres. The ADEPT tests were conducted in air at a pressure of 94 Torr at ambient room temperature using a 44-mm powder gun.

The HFFAF test section is 23 m long and has 16 orthogonal spark shadowgraph stations. The stations are evenly spaced every 1.524 m (5 ft) with all optical components external to the test section. The shadowgraph camera systems were recently upgraded from film to all digital cameras.[12] The time history of the model flight attitude and position are obtained from 16 pairs of shadowgraphs, from which aerodynamic coefficients can be inferred.[13] Example shadowgraph images of a model are shown in Figure 2. The pair of parallel lines seen in each image are wires. These are part of the fiducial reference system used to determine the model position and attitude.[14]

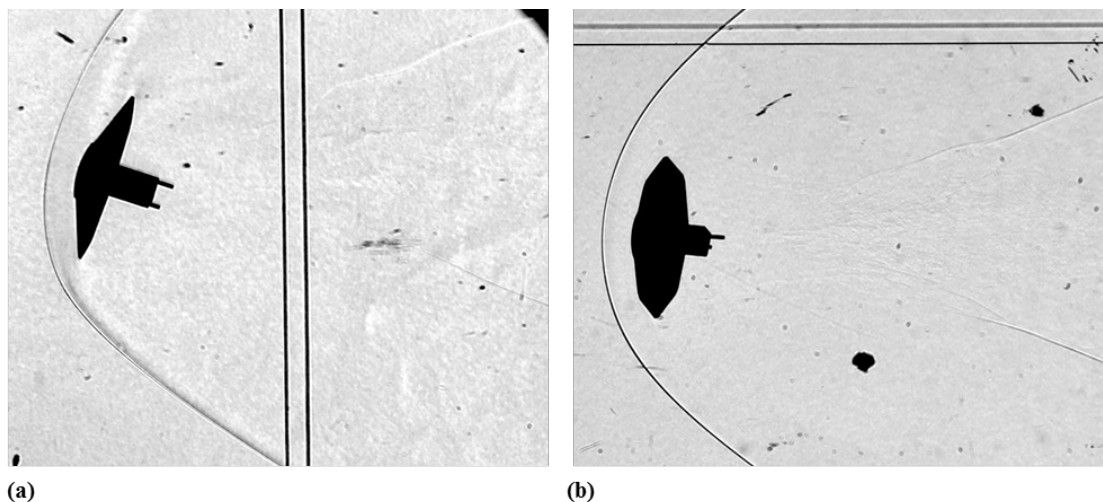(a)   (b)

Figure 2: Shadowgraph images of Nano-ADEPT in flight: (a) Pitch Plane; (b) Yaw Plane.

Each shot in a ballistic range experiment requires its own scaled model of the Nano-ADEPT geometry. Figure 3 shows a photograph of one pair of ballistic range models. The models were machined of titanium alloy (Ti-6Al-4V). The aft-body geometry was simplified, eliminating the structural details of the ribs, struts, and deployment mechanism of the flight vehicle, and representing the payload as a solid rectangle. As seen in the picture, a tungsten slug was placed near the end of the rectangular payload section to properly position the axial center of gravity. The model also included two aluminum pins on the base of the payload, which were used to measure the roll angle in the shadowgraph images. The position and attitude of the model were measured in each image by a template-matching method described in Bogdanoff *et al*,[12] with templates generated from the 3D-CAD model of the ballistic range model. This technique allowed roll angle to be determined without roll pins because of the faceted shape of Nano-ADEPT. Relative to the fiducial reference wires, measurement uncertainty was ± 0.25 mm for position and $\pm 0.3°$ for pitch and yaw angles. The positional accuracy along the full trajectory is estimated to be ± 3 mm. The accuracy of the reported values can be improved through further calibration, however, facility calibration for the new digital shadowgraph imaging systems was incomplete at the time of writing.
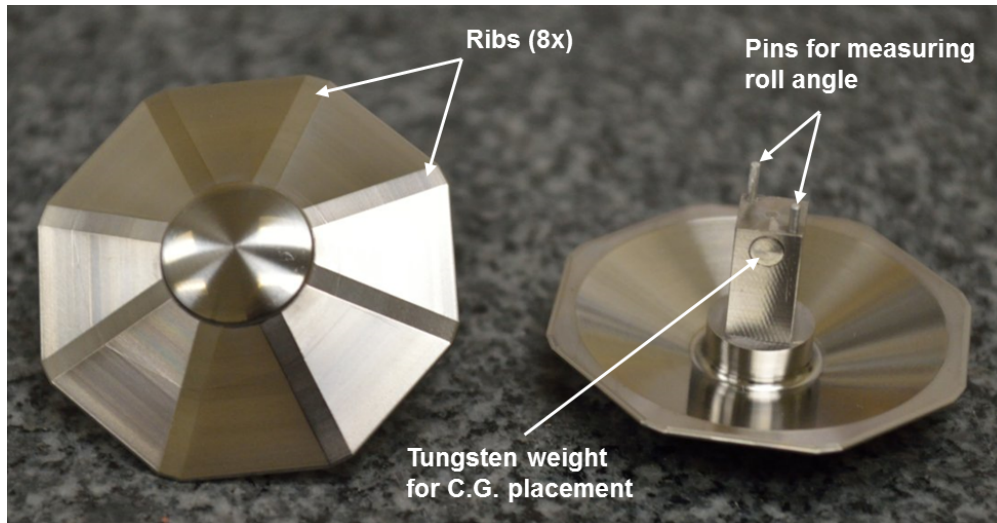
Figure 3: ADEPT SR-1 Ballistic Range Models, 3.56 cm diameter at rib tips.

The location of the center of gravity (CG) and the moments of inertia, I, about the principal axes, as shown in Figure 4, were measured for each model. The results are given in Table 1. The length of each model was measured with a precision micrometer. Additionally, the axial CG location was measured from the aft side of the payload and subtracted from the total length of each model, translating it to a location relative to the nose. The axial CG location was measured at least four times (y-axis up and down and z-axis up and down) to check for asymmetries, and averaged. Measured y_{cg} and z_{cg} offsets were less than the instrument accuracy and are considered to be zero. The quoted accuracy of the instrument is ± 0.003 cm for axial CG measurements, and ± 0.008 cm for off-axis measurements. Note that one model (shot 2783) did not have the tungsten weight in the payload section, and as a consequence, the axial CG location was closer to the nose. The coordinate system used in the ballistic range experiments can be seen in Figure 4. The moment of inertia about the y- and z-axes was measured at least twice for each, with the model rotated 180° between measurements to check for asymmetries. The moment of inertia about the x-axis was measured five times for each model with the model clocked at different angles about the x-axis relative to the instrument. The quoted accuracy of the instrument is ± 0.04 gcm^2.

Table 1: Ballistic range model dimensions and mass properties.

Shot	Model	D [cm] (at ribs)	L [cm]	Mass [g]	x_{CG} [cm]	x_{CG}/D	I_{xx} [g − cm²]	I_{yy} [g − cm²]	I_{zz} [g − cm²]
2783	unweighted	3.56	1.65	9.1131	0.514	0.144	9.03	5.51	5.5
2785	weighted	3.554	1.625	7.8258	0.561	0.158	6.75	4.55	4.55
2786	weighted	3.555	1.632	8.1054	0.56	0.158	7.12	4.66	4.66
2788	weighted	3.554	1.63	7.9562	0.559	0.157	6.92	4.64	4.65

All models were launched at a nominal zero-degree angle of attack, oriented in the gun with the z-axis up. Pitch oscillations were induced by impacting the lower half of the model with a sheet of material positioned at the entrance to the test section. The mass density of the sheet was used to control the amplitude of the resulting oscillations. The material used was either 0.5 mil Kapton, or one or more layers of 0.12 mil Mylar.

For launch, the model was packaged inside a segmented Nylon cylindrical carrier called a sabot, which was separated from the model by aerodynamic loads acting on the forward bevels of the sabot segments. Potential difficulties in launching these models were anticipated due to their unusual shape and low ballistic coefficient. Since the test was limited in scope, four low-cost prototype models were made to prove out the launch and separation. These prototype models did not include the tungsten CG weight or roll pins, and were machined at tolerances five times looser than typically required. These prototype shots revealed that
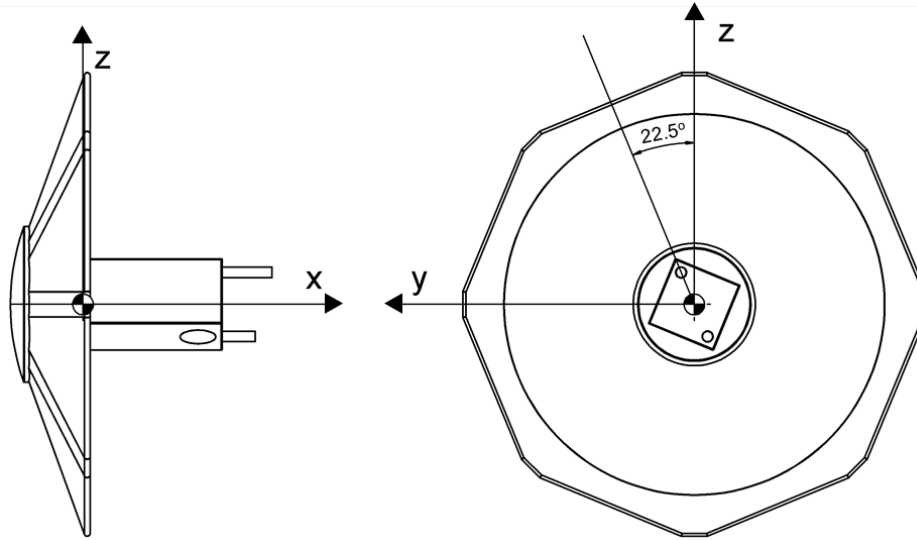
American Institute of Aeronautics and Astronautics

Figure 4: Coordinate system orientation for ballistic range experiments.

a minimum test gas pressure of $\sim$94 Torr was required to deflect the sabot segments and prevent them from entering the test section. One of the prototype shots, Shot 2783, yielded useful data.

B. Test Conditions

The goal of a ground test is to match the flight aerodynamics as well as the motion dynamics of the vehicle, thus achieving both aerodynamic and dynamic similarity. The average model velocity, test gas density, model size, and mass properties were selected to match the SR-1 flight conditions in terms of the following similitude parameters prioritized in this order:[15] the free-stream Mach number,

$$M = \frac{U_\infty}{a};$$ (1)

where U_∞ is the free-stream velocity. The freestream Reynolds number, Re_D, based on vehicle diameter, D,

$$Re_D = \frac{\rho_\infty U_\infty D}{\mu_\infty};$$ (2)

the dimensionless oscillation wavelength, λ,

$$\frac{\lambda}{D} = \sqrt{\frac{-C_{m,\alpha}\rho_\infty AD}{8\pi I}};$$ (3)

and the fractional velocity change over the distance of one pitch oscillation wavelength,

$$\frac{\Delta U}{U}|_\lambda = \frac{\rho_\infty C_D A\lambda}{2m};$$ (4)

where $C_{m,\alpha}$ is the derivative of the pitching moment coefficient with respect to angle of attack. The expected values of these parameters for the ADEPT SR-1 trajectory at $M = 1.2$ and 2.5 are given in Table 2 and the achieved test conditions are given in Table 3.

Table 2: Expected simultude parameters, ADEPT SR-1.

M	Re_D	$\frac{\lambda}{D}$	$\frac{\Delta U}{U}|_\lambda$	$V_\infty[\frac{m}{s}]$	$\rho_\infty[\frac{kg}{m^3}]$	C_D
1.2	123700	198	0.0251	372.6	0.0074	1.2
2.5	56900	412	0.0135	823.4	0.0017	1.35

Table 3: Achieved ballistic range test conditions.

Shot	Re_D	M_{avg}	$V_0[\frac{m}{s}]$	$\rho_\infty[\frac{kg}{m^3}]$	T_∞	$\frac{\lambda}{D}$	$\frac{\Delta U}{U}|_\lambda$
2783	136,000	1.38	534.2	0.1483	294.5	248	0.096
2785	124,000	1.23	487.5	0.1511	288.9	229	0.105
2786	123,000	1.21	480.0	0.1528	288.9	223	0.102
2788	235,000	2.36	893.64	0.1497	291.6	235	0.108

It is necessary to constrain λ_{test} due to the number and placement of shadowgraph stations such that the model executes between 1.5 and 3 cycles of motion along the test section. At least four well-defined peaks in the pitch oscillation waveform are necessary to determine whether the oscillation amplitude is damping or growing, and 5-6 samples (shadowgraphs) per cycle are needed to reliably define the peak amplitudes.[14] At the 94 Torr freestream pressure needed for sabot separation, it was not possible to achieve the low Reynolds number of the Mach 2.5 trajectory point. Tests at this condition, consequently, had a higher Reynolds number and a shorter oscillation wavelength than full-scale flight, as seen in Table 3.

C.   Geometry and Computational Grid

At moderate to low-supersonic regimes, the unsteady wake imparts significant moments on the vehicle. Adequately resolving the unsteady structures in the wake is crucial to accurately simulating free-flight dynamics. Utilizing a complex mesh topology and a simplified version of the geometry similar to the ballistic range model, a single high quality mesh was created to be used for all ballistic range conditions cited. The mesh itself contains over 55 million hexahedral elements. Nested refinement is used to aid in the capturing of relevant flow features in the near wake while maintaining computational efficiency. The local cell height in the near wake of the geometry is 0.5 mm. Like the ballistic range models, the surface geometry contains features deemed important to the study of the stability of the capsule, such as the paneled forebody, open back configuration, and the protruding payload structure on the aft-side of the craft. The computational geometry can be seen in Figure 5 and the computational mesh can be seen in Figure 6.

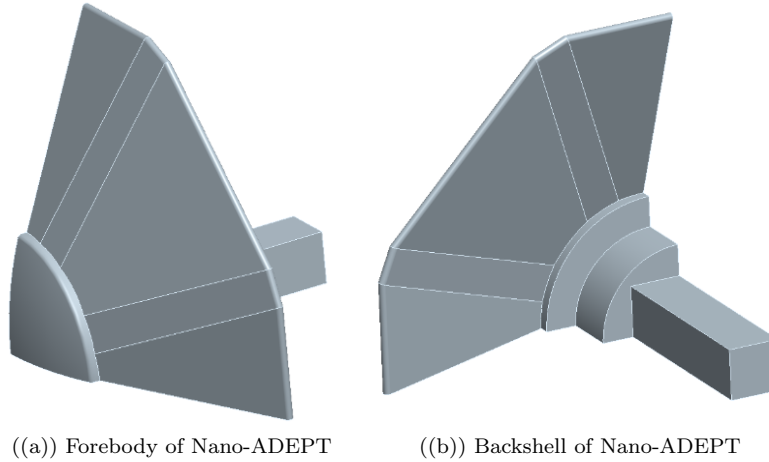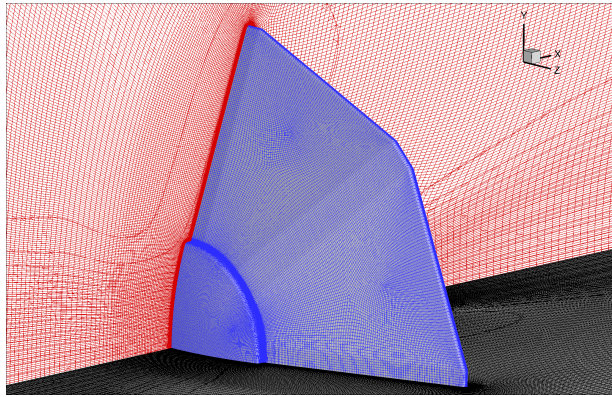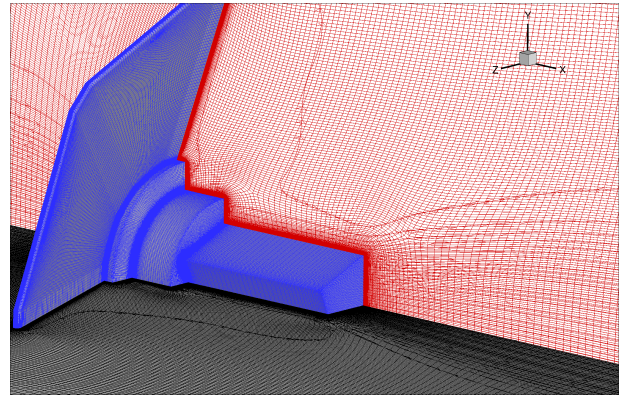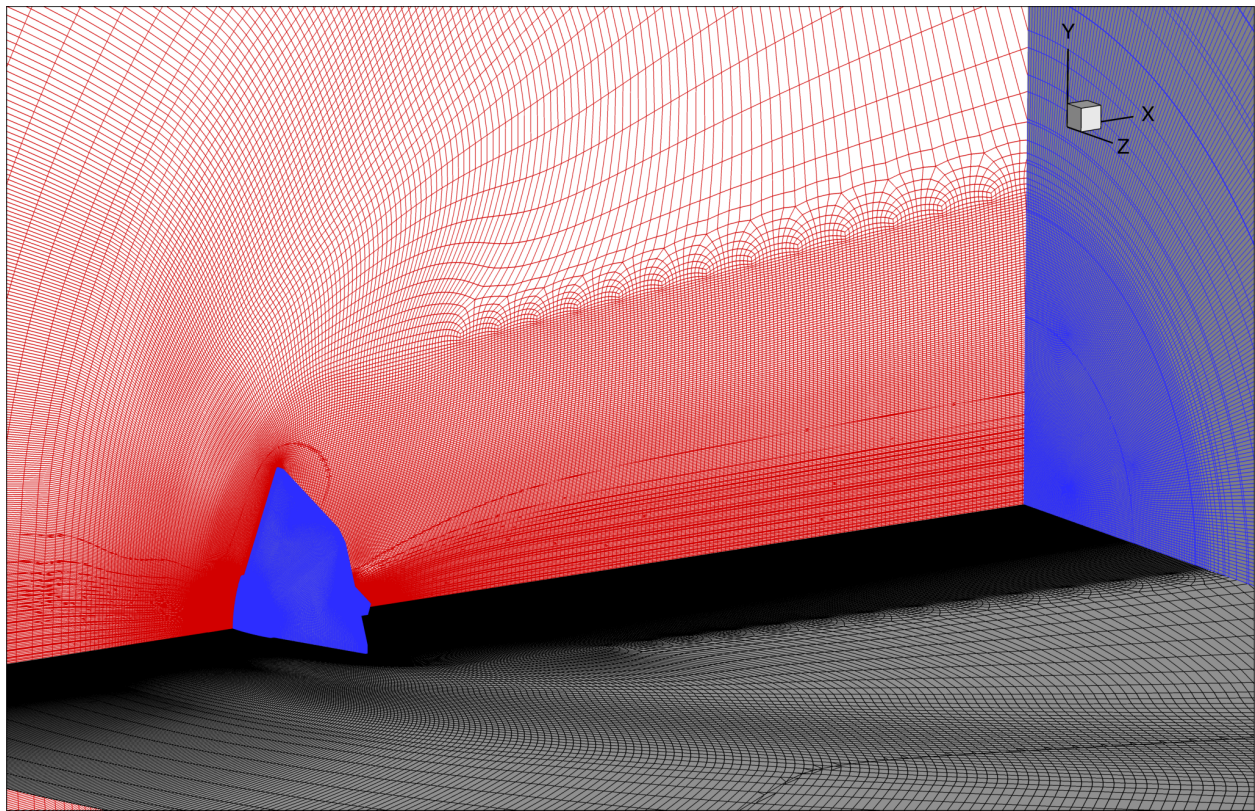((a)) Forebody of Nano-ADEPT   ((b)) Backshell of Nano-ADEPT

Figure 5: Computational Geometry.

(a) Computational Mesh Front-View

(b) Computational Mesh Aft-View

(c) Computational Mesh Front-View

Figure 6: Visualizations of the computational mesh used in ballistic range simulations.

American Institute of Aeronautics and Astronautics

D. Simulation Methodology

The flow solver used in this work, US3D, is an unstructured finite-volume Navier-Stokes flow solver originally developed at the University of Minnesota.[8] The unstructured implementation of US3D allows for complex mesh topologies to be exploited that improve the resolution of key features in the domain. For this work, spatial fluxes were solved using second-order low-dissipation fluxes in the Kinetic Energy Consistent (KEC) form formulated by Subbareddy *et al.*[16] For all simulations, the flow is assumed to be fully turbulent with turbulence modeling achieved using a hybrid Reynolds Average Navier-Stokes (RANS) and Large Eddy Simulation (LES) approach from the Detached Eddy Simulation (DES97) model developed by Spalart.[17] Time integration is performed using second-order Data Parallel Line Relaxation[18] (DPLR) in the near body of the vehicle, and second-order Full Matrix Point Relaxation (FMPR) scheme away from the body.

US3D also provides the capability to run dynamic simulations in 6-DOF. Rotational dynamics are modeled by mesh deformation in three distinct regions as seen in Figure 7. An inner region containing the surface geometry and near body flow-field is rigidly rotated in response to moments imparted by the flow onto the surface of the vehicle. An intermediate region linearly interpolates node displacements between the inner rotating region and outer static region. Translational dynamics are achieved by applying a frame velocity to the discrete equations.
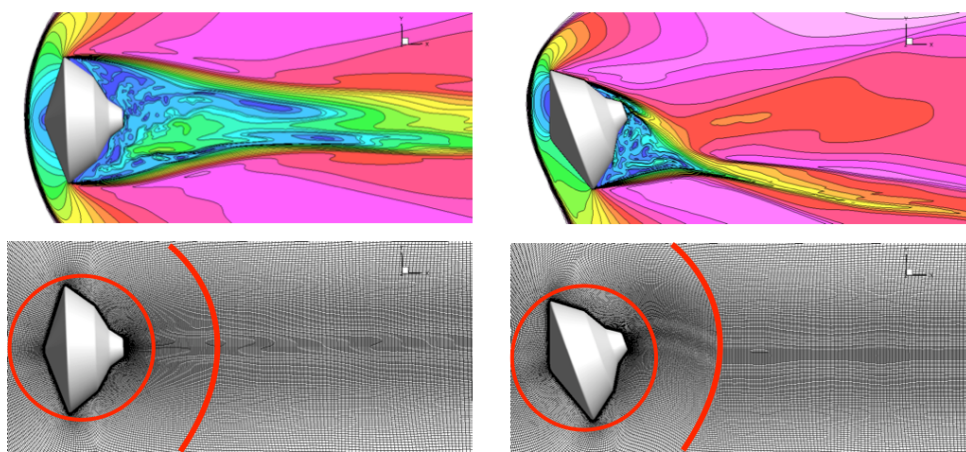

Figure 7: US3D Grid Deformation.[6]

The methodology for simulating free-flight behavior of the ballistic range Nano-ADEPT model will be similar to simulations of the Supersonic Inflatable Aerodynamic Decelerator (SIAD) completed by Brock *et al.*[5] The first step of simulating free-flight ballistic range models is to initialize the flow-field at a static vehicle attitude corresponding to the first experimental data point. The free-stream conditions, model attitude, and model mass properties match the conditions given by the ballistic range experiments, given above in Table 3. The simulation runs continuously to wash out any transients due to startup and the forces and moments converge to a quasi-steady value. Snapshots from the initialized flow-field of Shot 2783 can be seen in Figure 8. The top two plots show u-velocity and temperature contours respectively, while the bottom plot shows iso-surfaces drawn according to the Q-criterion, an objective measure to visualize turbulent flow-fields given by Equation 5,

$$Q = -\frac{1}{2}(S_{ij}S_{ij} - \Omega_{ij}\Omega_{ij}) = -\frac{1}{2}\frac{\partial u_i}{\partial u_j}\frac{\partial u_i}{\partial u_j} \tag{5}$$

Where

$$S_{ij} = \frac{1}{2}(\frac{\partial u_i}{\partial u_j} + \frac{\partial u_i}{\partial u_j}), \ \Omega_{ij} = \frac{1}{2}(\frac{\partial u_i}{\partial u_j} - \frac{\partial u_i}{\partial u_j}) \tag{6}$$

Following flow-field initialization, initial rotation and translation rates are applied to the simulated model. Rotation rates were calculated by fitting a sinusoidal function to the ballistic range data and computing the slope at the first data point. Additionally, translational velocities were calculated using a linear approximation of the slope between the first two data points from the ballistic range and applied as a frame velocity.
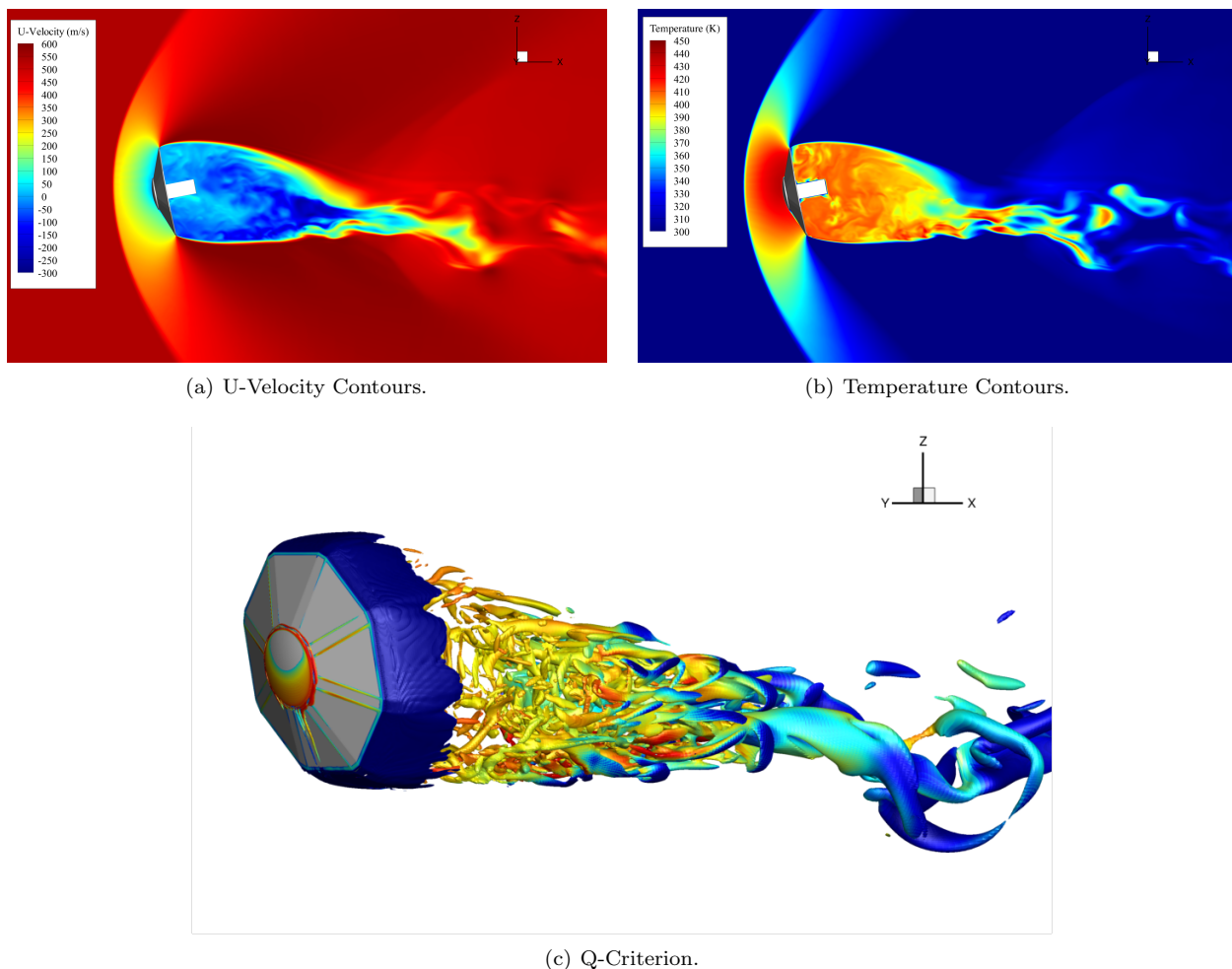
American Institute of Aeronautics and Astronautics

(a) U-Velocity Contours.

(b) Temperature Contours.

(c) Q-Criterion.

Figure 8: Shot 2783 Flow Initialization.

E.   Ballistic Range Simulation Results

1.   Comparison of Simulation to Experimental Data

In this section, we compare predicted dynamics from US3D to data from the experiment. The ballistic range simulations can be seen arranged in rows of increasing Mach number in Figure 9. The far left plot shows the pitch and yaw angle vs time, the center plot shows downrange distance vs time, and the far right plot shows total angle-of-attack vs time. The total angle-of-attack is defined in Equation 7.

$$\alpha_T = cos^{-1}(cos(\alpha)cos(\psi)) \tag{7}$$

The error in pitch, yaw, and total angle-of-attack measurements are taken to be the measurement error from the ballistic range experiments, $\pm 0.3°$. The highest Mach number case, Shot 2788 (last row, Figure 9), shows excellent agreement with experiment data in all three categories. This is a similar level of accuracy as was seen in Brock *et al.*[5] during the simulation of similar Mach regions using the SIAD geometry. To extend into the lower Mach number regime, we will examine Shot 2785 (second row, Figure 9). This case compares well with experimental data in downrange distance, indicating that the aerodynamic drag is being represented correctly in the CFD simulations. The frequency of oscillation also matches experiment, but there is a discrepancy in peak amplitude between CFD and experiment that results in a $\sim 2.5 - 3.0°$ (10%) difference. This trend is a consistent result across computed trajectories with an average Mach number under 1.5 and results in an average under-prediction in peak amplitude of $\sim 16\%$.
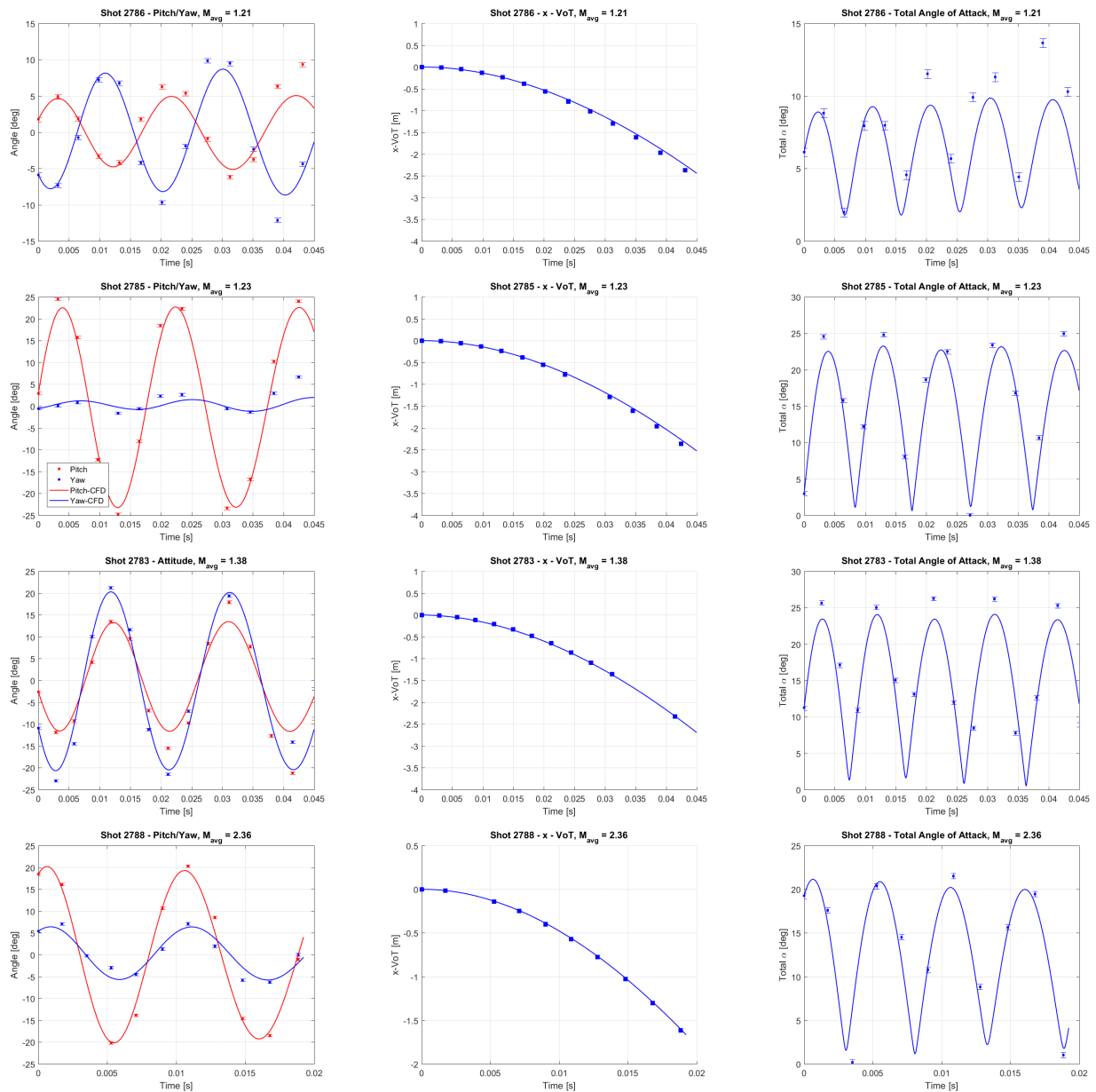
American Institute of Aeronautics and Astronautics

Figure 9: Ballistic Range Simulation Attitudes.

2. Investigation of Surface Pressure

An advantage of using CFD to simulate flight conditions is the ability to interrogate the flow in ways that would be prohibitively difficult to perform in an experiment. Taking advantage of this capability, additional information into fluid-vehicle response coupling and its dependence on Mach number can be investigated. A plot of the pressure coefficient at the forebody stagnation point and a point on the aft of the payload of Shot 2788 can be seen in Figure 10.

The forebody stagnation pressure coefficient of Shot 2788 smoothly oscillates and decreases from approximately 1.65 to 1.15 because of the decrease in dynamic pressure caused by the vehicle's deceleration. The aft-body pressure signal is noisier, but oscillates and increases between -0.155 and -0.135. Figure 11 shows the pressure coefficients from the lowest Mach number case, Shot 2786. This simulation shows a similar pattern, but the forebody pressure coefficient decreases from approximately 1.5 to 0.7, while the aftbody pressure coefficient increases from -0.3 to -0.22. The difference between the absolute value of fore and aft-
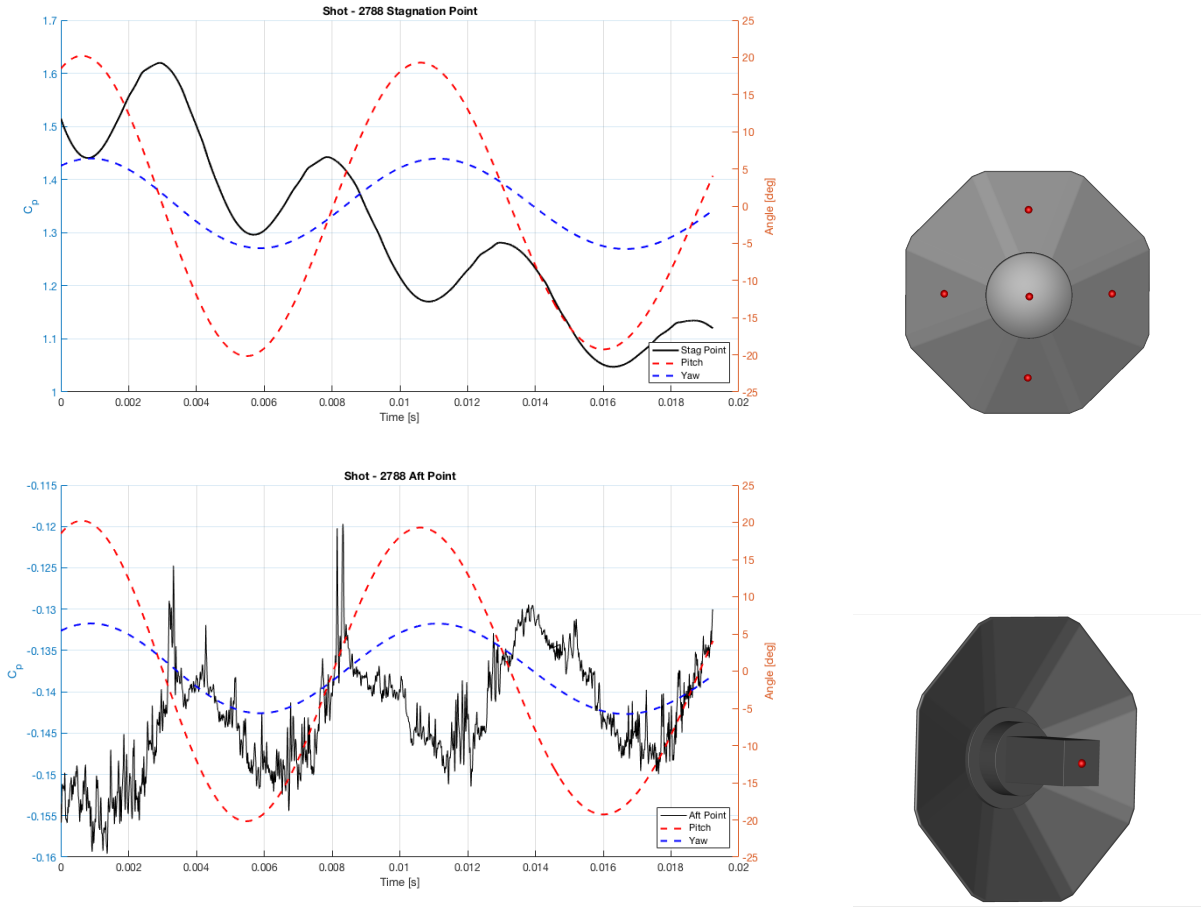
American Institute of Aeronautics and Astronautics

Figure 10: Shot 2788 Pressure Coefficients ($M_{avg} = 2.36$).

body pressure coefficients is larger in the higher Mach number case. This means that the forebody moment contribution dominates due to higher pressure values seen on the forebody as compared to pressure values seen on the aftbody at high Mach numbers. As the Mach number decreases, the difference in magnitude between the fore and aftbody pressure coefficients becomes smaller and the moment contribution generated on the aftbody has a larger influence on vehicle dynamics. This is a general trend and suggests that unsteady flow structures in the wake become more important at lower Mach numbers, placing an emphasis on proper wake resolution and numerics. This trend is consistent with the findings of Brock *et al.*[5]
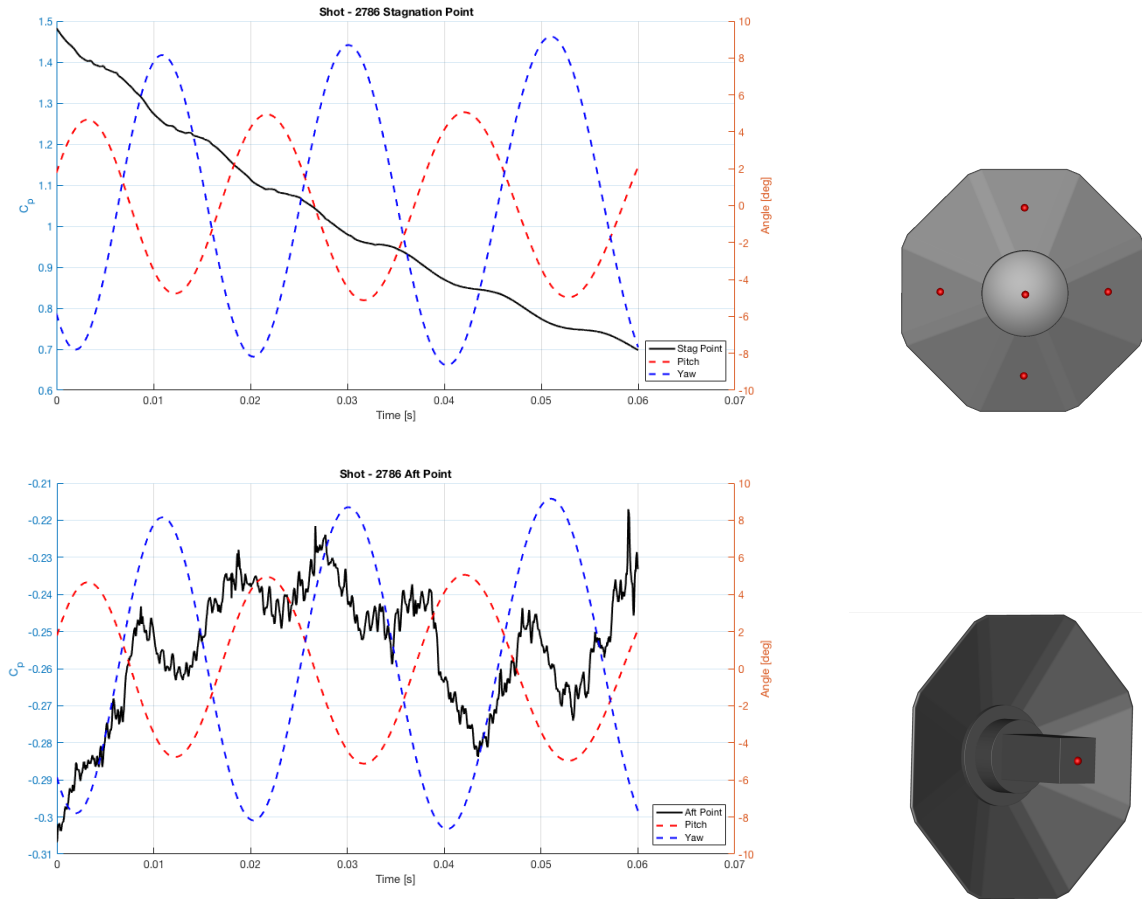
American Institute of Aeronautics and Astronautics

Figure 11: Shot 2786 Pressure Coefficients ($M_{avg} = 1.21$).

Figure 12 shows traces of pressure coefficient located half way between the nose cone interface and the edge of the deployed heat shield on the forebody of the vehicle. The probes are oriented at $90°$ intervals about the axis of rotational symmetry starting and labeled as numbers on a clock face. Looking at the 12 and 6 o'clock probes, we see the pressure rise and fall are closely coupled to the in-phase oscillation of the vehicle's pitch and yaw attitudes. The 12 o'clock probe sees its maximum pressure coefficient when pitch and yaw are at their maximum, while the 6 o'clock probe sees its maximum when the pitch and yaw are at a minimum. Additionally, the pressure probe located on the windward side (12 o'clock probe at high pitch and 6 o'clock probe at low pitch) experiences pressure fluctuation due to the flow separating over a backward facing step. Figure 13 shows flow separation and reattachment that comes from the backward facing step between the nose cap and heat shield panels using the Q-criterion, an objective method used to detect and visualize vortices. By following a stagnation point streamline that diverges up toward the 12 o'clock probe on left side of Figure 13, we can see that the separated region contains an unsteady vortex that may feed fluid from the windward side of the forebody, around the nose cap, and down to the leeward side. Furthermore, the favorable pressure gradient from the windward to leeward side around the nose cap may be stabilizing the flow, resulting in the relatively small fluctuations seen in the pressure traces.
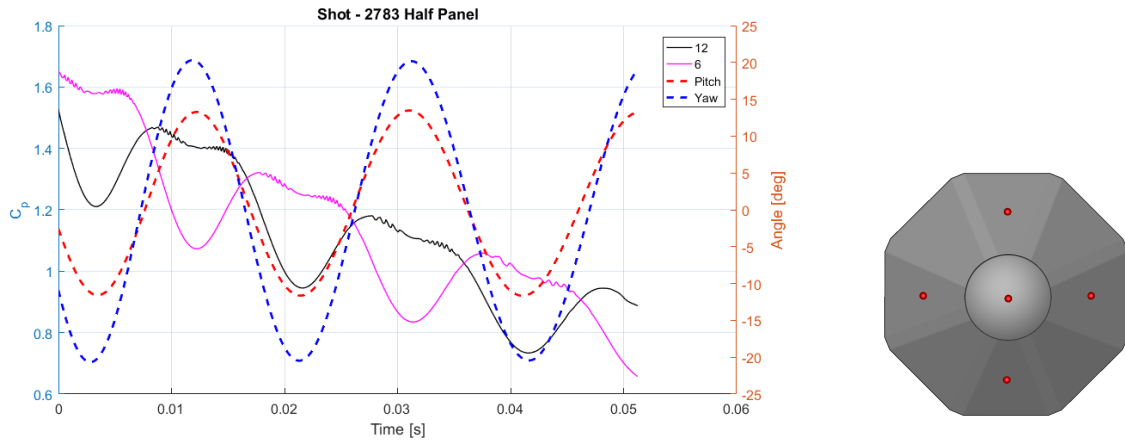
American Institute of Aeronautics and Astronautics

Figure 12: Pressure coefficients halfway between the nose cap and heat shield edge - Shot 2783.

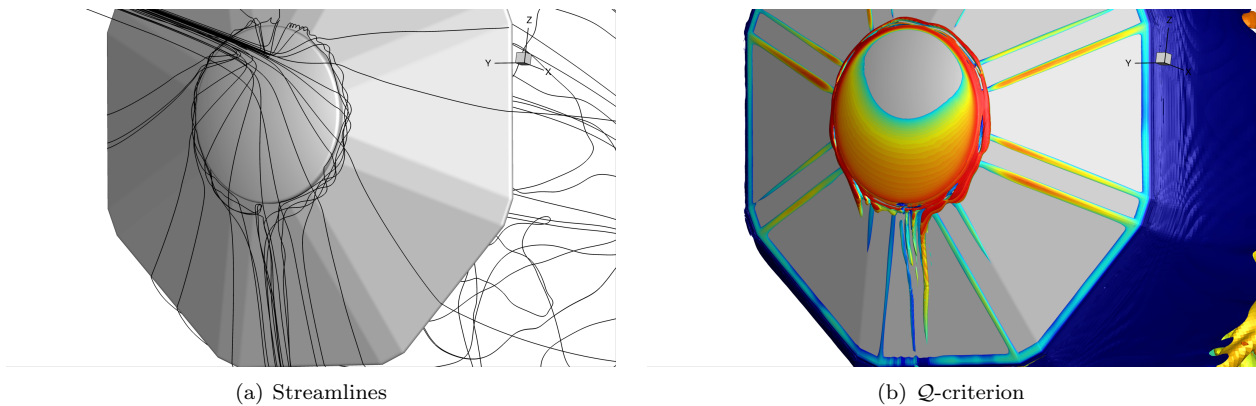(a) Streamlines

(b) $\mathcal{Q}$-criterion

Figure 13: Visualization of forebody flow separation on nose cap for Shot 2783.

IV. Flight Trajectory Simulation

A. Simulation Methodology

In previous presentations, the dynamics solver within US3D could only perform free-flight simulations at a single free-stream condition; it could not simulate a full trajectory with changing atmospheric conditions. The solver was limited to one thermodynamic (temperature and pressure) free-stream condition per simulation, which is not representative of atmospheric descent. This is especially true in the case of ADEPT SR-1, where the capsule descends through the atmosphere at a near-vertical flight path angle through a rapid and substantial variation of atmospheric conditions. In order to perform a flight-relevant simulation of SR-1, this work looks to add the capability to change the free-stream values in response to the translational and rotational dynamics "on-the-fly".

The scope of this section is to present a "proof-of-concept". While there is a sounding rocket test planned in the future, there is no experimental data available to compare with the results of this section's simulations. This makes it difficult to make conclusions regarding the accuracy of the numerics beyond the confidence built from the ballistic range comparisons in the previous section. Furthermore, because the accuracy of the presented simulations needs further verification, this section will not attempt to assess the stability characteristics of the Nano-ADEPT geometry; it is only being used as a test case. As a result, this section will give an overview of the simulation method as well as some of the unique challenges associated with flight-scale trajectory simulations using CFD.

American Institute of Aeronautics and Astronautics

In a flight test, the capsule starts at an initial attitude, flight-path angle, and altitude in a certain planetary atmosphere. To this end, the developed algorithm takes inputs of the initial velocity vector (v), capsule geometry, attitude, and altitude (h). Given this information, an atmospheric model is used to calculate the free-stream boundary conditions at each time step. These are then used to update the inflow, after which, the solver resolves the flow and takes a time step. Subsequently, the velocities calculated by US3D's dynamics solver are used to update the altitude and the loop repeats. The process is shown in Algorithm 1.

Algorithm 1 Trajectory Simulation Using CFD

1: **procedure** BOUNDARY CONDITION UPDATE
2: *loop*:
3:     *Inflow* $\leftarrow \rho_\infty(h)$ *and* $T_\infty(h)$
4:     Solve flow at the current time-step.
5:     Update the capsule velocity $v(t)$ with information from the dynamics solver.
6:     Take a time-step: *dt*.
7:     $h_t \leftarrow h_{t-1} - v_{t-1}dt$.
8:     **goto** *loop*.

In order to execute these steps, the solver needs to automatically update the inflow boundaries of the domain with the proper free-stream boundary conditions using an appropriately selected atmospheric model. The chosen variables of interest are the free-stream density (ρ_∞) and temperature (T_∞). From these, all of the thermodynamic variables can be calculated and the flow solution can be updated. Because the craft is flying at mid to low supersonic speeds, the gas is assumed to be non-reacting and the atmosphere is assumed to be composed of a perfect gas, air. To represent the atmosphere, this work uses the 1976 Standard Atmosphere Model for simplicity.

A separate grid was developed for use in the trajectory simulations. Unlike the ballistic range mesh, this grid was a flight-scale version of the simplified Nano-ADEPT geometry. The diameter of the forebody was 0.7 m rib-tip to rib-tip and the length of the capsule was 0.32 m. The full computational mesh contains ~ 23 million hexahedral elements. The mesh in the wake utilized the same nested-refinement topology as in the ballistic range case, but the maximum cell height is 1 cm. The surface grid with its associated pressure probes can be seen in Figure 14.
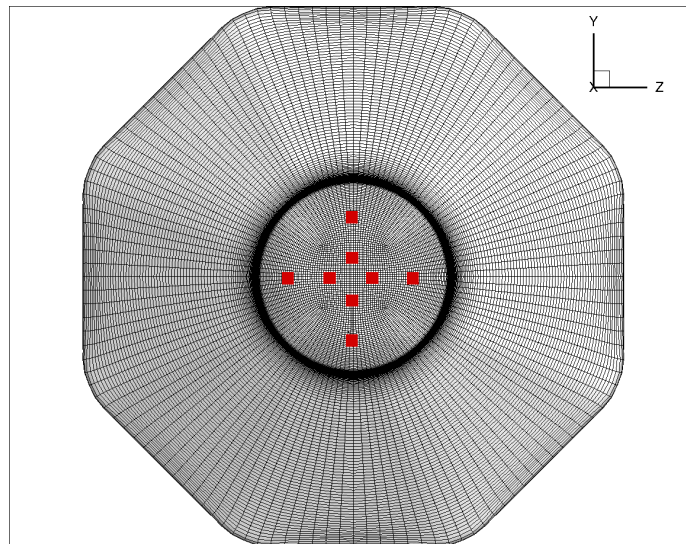

Figure 14: Trajectory Simulation Forebody Surface Grid.

Due to constraints on computational resources and near-wall grid spacing, the trajectory simulations were split into two segments. In order to ensure proper resolution of the boundary layer during simulation, near wall grid cells must be properly spaced. This wall spacing requirement is driven by the Reynolds number of the flow field; a quantity that is constantly changing throughout a trajectory. High in the atmosphere where

American Institute of Aeronautics and Astronautics

the Reynolds number is lower, a larger wall spacing can be used to refine the boundary layer. Lower in the atmosphere, the Reynolds number is higher and requires more grid cells near the wall to resolve properly. Thus, wall spacing during early descent requires less refinement than wall spacing during late descent given the $y^+ \leq 1$ requirement.[19] The tighter spacing requirements due to the high Reynolds number seen during the lower portion of descent places a limit on the time step to be taken during the higher-altitude portion of descent because of mesh over-refinement near the wall. As a result, two different mesh spacings near the wall were utilized for two unconnected portions of the trajectory, changing the cell count by less than 1% between the two trajectory simulations. One simulation took place during the high-speed and high-altitude portion of descent and the other took place during the lower-speed and low-altitude portion of descent.

For both trajectory simulations, the initialization was done in much same way as in the ballistic range cases. Numerical settings within US3D used in the trajectory simulations are the same as they were in the ballistic range simulations. However, instead of assigning free-stream conditions, the initial conditions are calculated with the 1976 Atmosphere using the expected altitude and Mach number given by the most current POST2[20] simulation of the expected flight trajectory. Moreover, initial vehicle attitude was chosen to be of a magnitude that would excite the oscillatory dynamics of the capsule. The simulation was then allowed to run statically using values from Table 4 to wash out transients due to startup. Additionally, the forces and moments acting on the capsule were allowed to converge to quasi-steady values. Following flow-field initialization, the routine is initialized using the flight-path angle, altitude, and velocity given in Table 4, as well as mass properties described in Table 5. The capsule is then ready to be "released" in order to simulate the trajectory.

Table 4: Initialized values for the CFD trajectory simulations.

	Simulation 1 - High Altitude	Simulation 2 - Low Altitude
$V_0 \ [\frac{m}{s}]$	978.6	379.9
Flight Path Angle [°]	-89.2	-89.7
Pitch, Yaw, and Roll Angle [°]	(15, 0, 0)	(15, 0, 0)
Altitude [km]	53.5	36.2
Mach Number Range	3.0-2.6	1.22-0.89
Re_D	26,000-46,000	115,000-119,000
Wall Spacing Requirement [m]	4.6e-04	1.2e-04

Table 5: Mass properties of the simulated full-scale Nano-ADEPT model.

Mass [kg]	x_{CG}/D	I_{xx} [$kg-m^2$]	I_{yy} [$kg-m^2$]	I_{zz} [$kg-m^2$]	I_{xy} [$kg-m^2$]	I_{xz} [$kg-m^2$]	I_{yz} [$kg-m^2$]
9.94	0.157	0.298	0.189	0.189	-0.0004	-0.0001	-0.0002

B.   High Altitude

Figure 15(a) shows the Mach number and density vs altitude results for the high-altitude portion of descent. As the Nano-ADEPT descends through the atmosphere, evidence of deceleration can be seen due to the aerodynamic drag forces, demonstrating that the new routine is tracking the vehicle's trajectory. The free-stream density is increasing, as it should be according to the 1976 Atmosphere, indicating that the simulation is correctly changing the boundary conditions as the simulation runs. Figure 15(b) shows density contours on the symmetry plane of the capsule at the beginning of this trajectory segment. The capsule is oriented downward and in the direction of flight. The flow field exhibits features characteristic to blunt-body supersonic flight. The forebody is dominated by a strong and detached bow shock. Additionally, due to the open back design of the vehicle, the flow separates off of the back of the deployed heatshield and results in a separation bubble behind the vehicle. Finally, the flow re-accelerates to supersonic speeds around the wake and experiences a recompression shock.

American Institute of Aeronautics and Astronautics

((a)) Altitude and Density vs. Mach
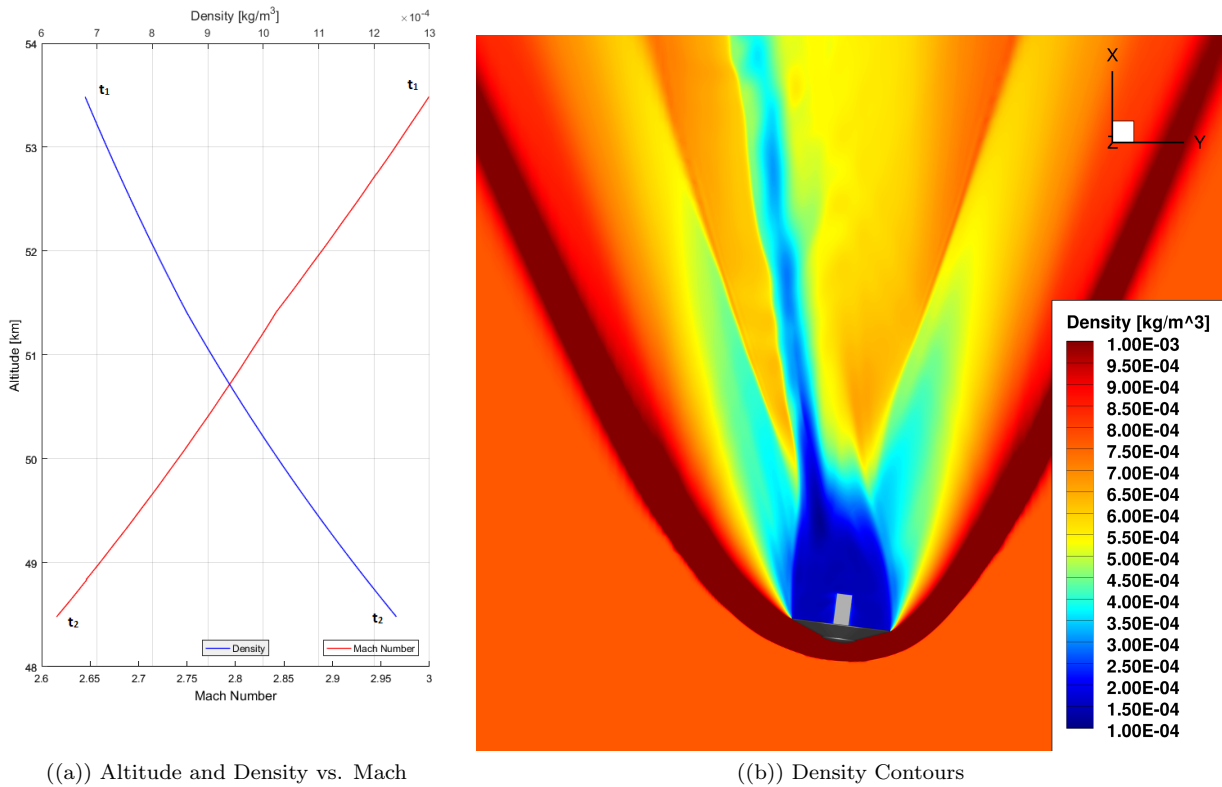
((b)) Density Contours

Figure 15: Simulation of Nano-ADEPT during high-altitude flight.

Pressure probe data can be seen in Figure 16. Like in the ballistic range simulations, solution probes were placed around the axis of rotation on planes coinciding with 90° increments starting on the vertical axis of symmetry (12 o'clock) in order to assess dynamic forcing. The craft sees an increase in pressure throughout descent even though it is decelerating. This is to be expected because the increase in ambient pressure is increasing faster than the decrease in dynamic pressure within this trajectory segment. Additionally, the spikes seen around the pressure peaks are numerical artifacts caused by large grid deformations in the presence of a strong shock wave. Strategies to mitigate this effect are the subject of future work.
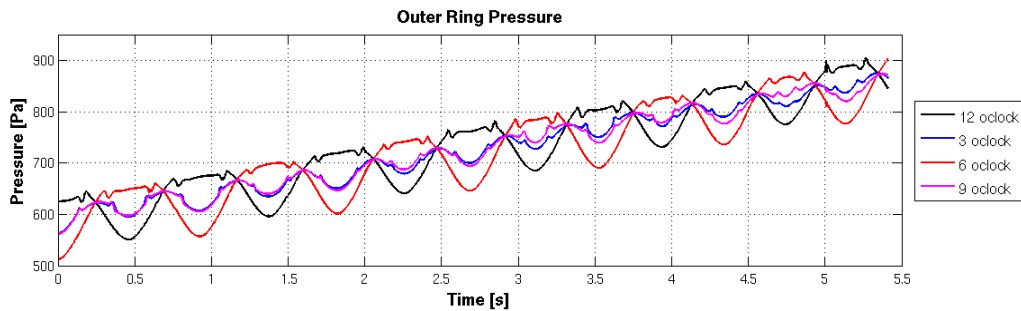

Figure 16: Forebody pressure during high-altitude descent.

Figure 17 shows the vehicle's attitude information through the first trajectory segment. The first plot shows pitch attitude vs time, the second plot shows yaw attitude vs time, and the final plot shows total angle-of-attack vs time. These plots demonstrate the new routine's ability to simulate and track attitude information during atmospheric descent through many cycles of oscillation. According to the plots, both pitch angle and total angle-of-attack are decreasing in this portion of the trajectory.
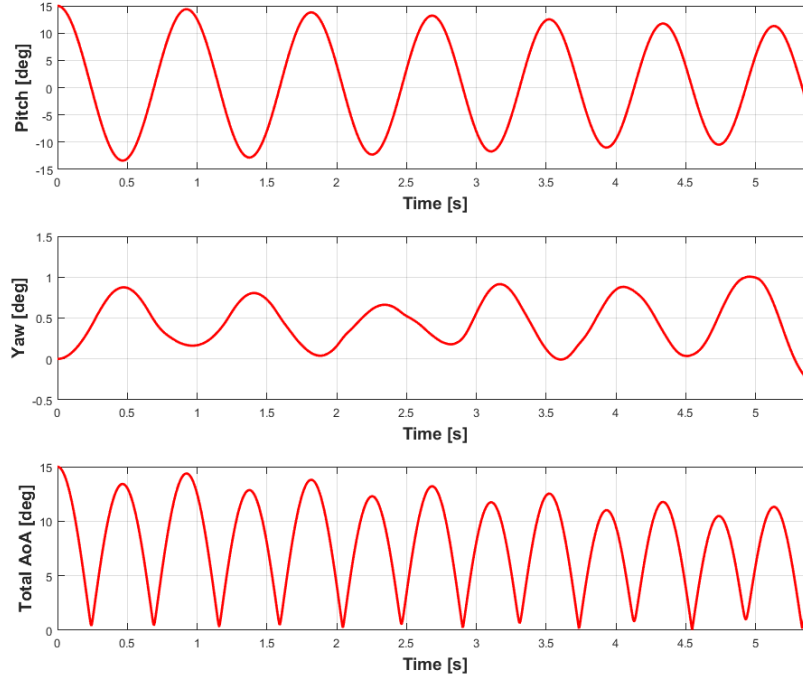
American Institute of Aeronautics and Astronautics

Figure 17: Attitude information from the CFD trajectory simulation of the Nano-ADEPT during high altitude descent.

C.   Low Altitude

Figure 18(a) shows the Mach number and density vs altitude plot during the lower portion of descent. Furthermore, it demonstrates the routine's ability to track the altitude and Mach number of the vehicle through the transonic flight region. Figure 18(b) shows density contours of the near-body flow field during the beginning of the lower trajectory segment. Note that the atmospheric (free-stream) density in this portion of descent is 10 times higher than it was in the high-trajectory segment. Similar to the high altitude case, a bow shock is present off of the forebody of the vehicle. This shock sits at a larger stand-off distance and indicates that the craft has decelerated as compared to the speeds seen during high-altitude descent. Moreover, smaller flow structures in the wake are apparent; a typical result of higher Reynolds number flow. Evidence of a reflected shock in the wake can be seen behind the shock on the left side of the contour plot. Because the computational domain was sized for the first trajectory segment's shock placement, the shock impinges upon the boundaries of the mesh, causing a numerical reflection. Mitigating this issue for full trajectory spaces is a topic of future work. Figure 19 shows the attitude information from the lower-trajectory portion of descent similarly to Figure 17. The plots show growth in pitch angle, yaw angle, and total angle-of-attack in this portion of the trajectory. Again, the plots demonstrate the routine's ability to simulate many cycles of the vehicle's oscillatory dynamics throughout the lower-trajectory segment.

American Institute of Aeronautics and Astronautics
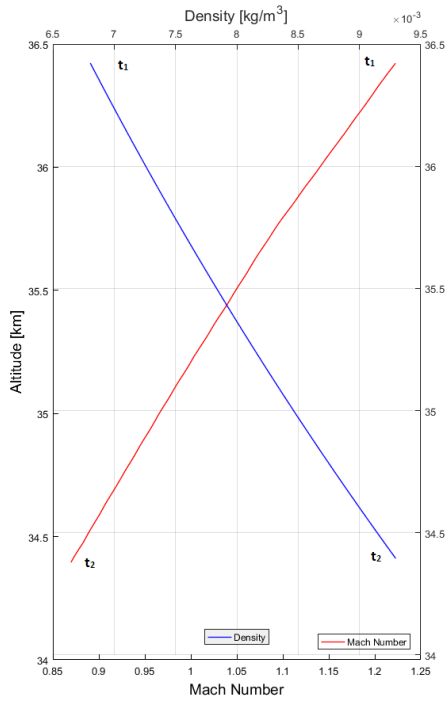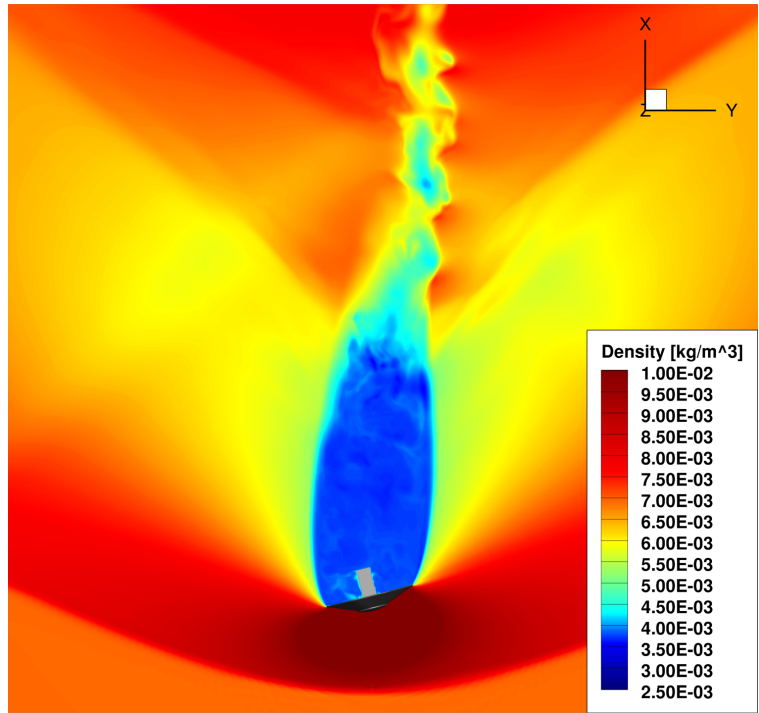
((a)) Altitude and Density vs. Mach   ((b)) Density Contours

Figure 18: Simulation of Nano-ADEPT during low-altitude flight.
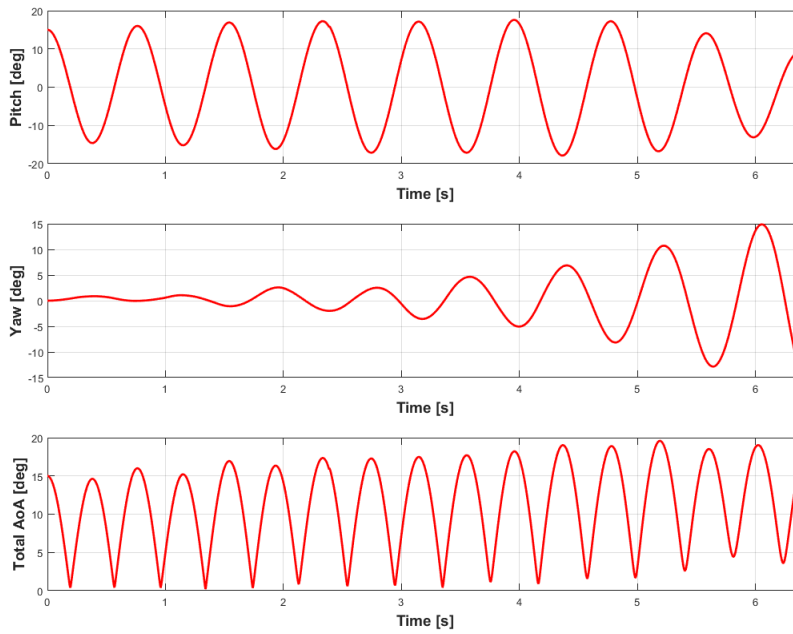

Figure 19: Attitude information from the CFD trajectory simulation of Nano-ADEPT during low altitude descent.

D. Computational Time

The time scales associated with typical CFD simulations are small in magnitude. To simulate a flight trajectory, a much longer run time is required. The ADEPT SR-1 mission spans a total flight time of 40 seconds. Because we desire to simulate the full trajectory, these simulations have the potential to place a large demand on computational resources. The simulations presented here span 5.5 and 6.5 seconds of their respective portions of the full trajectory. As seen in Table 6, it took 5 days to simulate each trajectory segment. These were simulated using 256 cores on a local computer cluster. It would take 36 days to run the full trajectory based on the simulation time from the high altitude simulation. Moreover, to properly resolve relevant flow features, such as the separation about the nose cap and the unsteady wake dynamics, the grid resolution likely needs to be increased. All things considered, the simulations could be run on a larger computer cluster to offset some of the computational demands. If we assume that increasing the number of computing cores to 1024 decreases the amount of run time for each simulation by 4 times, and assume that doubling the grid size doubles the computational time, a full-scale time-accurate simulation of the SR-1 mission could be achieved in 14 days.

Table 6: Computational Demand of ADEPT SR-1 Trajectory Simulations.

	Simulation 1 - High Altitude	*Simulation 2 - Low Altitude*
Mach Number Range	3.0-2.6	1.22-0.89
Flight Time - Simulation	5.5 seconds	6.5 seconds
Reynolds Number Range	26,000-46,000	115,000-119,000
CPU Time	1,280 Days	1,280 Days
Wall Time	5 Days	5 Days

V.   Conclusions and Future Work

A computational study of the ADEPT SR-1 flight article was performed. The desire to simulate this experiment using CFD requires a methodology that is capable of changing the free-stream conditions throughout the simulated descent because the atmospheric density associated with the trajectory of ADEPT SR-1 changes by more than a factor of 10 throughout the flight experiment. In order to provide an assessment of the validity of performing trajectory simulations using high-fidelity CFD, a comparison with ballistic range experiments of the ADEPT SR-1 geometry was completed using US3D.

When compared to experiment, the ballistic range simulations of Nano-ADEPT showed excellent agreement to experimental pitch, yaw, and downrange distance in the high Mach number case ($M_{avg} = 2.36$). When the simulation methodology was extended to Mach numbers below 1.5, downrange distance and oscillatory frequency were correctly predicted, but the peak oscillatory amplitude of total angle-of-attack was under predicted by an average of $\sim 16\%$.

Building upon the ballistic range simulations, full-scale trajectory simulations of ADEPT SR-1 using US3D were also presented. The trajectory simulations of the full-scale mission utilized US3D's free-flight capability coupled with the 1976 Atmosphere to predict relevant trajectory information while changing free-stream conditions. A "proof-of-concept" study was presented and the method's ability to track and predict a capsule's attitude, position, velocity, and pressure information during a planetary EDL mission was demonstrated. In addition, challenges with mesh generation due to changing wall spacing requirements and shock position were identified. In order to run full flight-relevant trajectories in the future, a novel gridding strategy such as adaptive mesh refinement should be developed and implemented. Furthermore, full time-accurate flight-scale trajectory simulations were shown to be computationally demanding, requiring two weeks to complete in the case of ADEPT SR-1 given adequate computing resources.

Free-flight simulations using CFD continue to show promise in the prediction of entry vehicle dynamics, but further verification is needed in order to properly characterize them as a flight predictor. Further characterization will be achieved through additional ballistic range comparisons and a one-to-one comparison study using data from the SR-1 flight experiment in future work.

American Institute of Aeronautics and Astronautics

Acknowledgements

References

[1]Venkatapathy, E., Hamm, K., Fernandez, I., Arnold, J., Kinney, D., Laub, B., Makino, A., McGuire, M., Peterson, K., Prabhu, D., Empey, D., Dupzyk, I., Huynh, L., Hajela, P., Gage, P., Howard, A., and Andrews, D., "Adaptive Deployable Entry and Placement Technology (ADEPT): A Feasibility Study for Human Missions to Mars," *21st AIAA Aerodynamic Decelerator Systems Technology Conference and Seminar*, American Institute of Aeronautics and Astronautics, Dublin, Ireland, May 2011.

[2]Smith, B., Yount, B., Kruger, C., Brivkalns, C., Makino, A., Cassell, A., Zarchi, K., McDaniel, R., Ross, J., Wercinski, P., et al., "Nano-ADEPT Aeroloads Wind Tunnel test," *IEEE Aerospace Conference Proceedings 2015*, IEEE, Big Sky, MT, 2016, pp. 1–20.

[3]Kazemba, C. D., Braun, R. D., Schoenenberger, M., and Clark, I. G., "Dynamic Stability Analysis of Blunt-Body Entry Vehicles Using Time-Lagged Aftbody Pitching Moments," *Journal of Spacecraft and Rockets*, Vol. 52, No. 2, March 2015, pp. 393–403.

[4]Schoenenberger, M., Yates, L., and Hathaway, W., "Dynamic Stability Testing of the Mars Science Laboratory Entry Capsule," *41st AIAA Thermophysics Conference*, American Institute of Aeronautics and Astronautics, San Antonio, TX, June 2009.

[5]Brock, J. M., Stern, E., and Wilder, M. C., "Dynamic CFD Simulations of the Supersonic Inflatable Aerodynamic Decelerator (SIAD) Ballistic Range Tests," *55th AIAA Aerospace Sciences Meeting*, American Institute of Aeronautics and Astronautics, Grapevine, TX, January 2017.

[6]Stern, E., Gidzak, V., and Candler, G., "Estimation of Dynamic Stability Coefficients for Aerodynamic Decelerators Using CFD," *30th AIAA Applied Aerodynamics Conference*, American Institute of Aeronautics and Astronautics, New Orleans, LA, June 2012.

[7]Stern, E., Schwing, A., Brock, J. M., and Schoenenberger, M., "Dynamic CFD Simulations of the MEADS II Ballistic Range Test Model," *AIAA Atmospheric Flight Mechanics Conference*, American Institute of Aeronautics and Astronautics, San Diego, CA, June 2016.

[8]Nompelis, I., Drayna, T., and Candler, G., "A Parallel Unstructured Implicit Solver for Hypersonic Reacting Flow Simulation," *17th AIAA Computational Fluid Dynamics Conference*, American Institute of Aeronautics and Astronautics, Toronto, ON, CA, June 2005.

[9]Smith, B., Cassell, A., Kruger, C., Venkatapathy, E., Kazemba, C., and Simonis, K., "Nano-ADEPT: An entry system for secondary payloads," *IEEE Aerospace Conference Proceedings 2015*, Big Sky, MT, 2015.

[10]Wercinski, P., Smith, B., Yount, B., Cassell, A., Kruger, C., Brivkalns, C., Makino, A., Dutta, S., Ghassemieh, S., Wu, S., Battazzo, S., Nishioka, O., and Venkatapathy, E., "ADEPT Sounding Rocket One (SR-1) Flight Experiment Overview," *IEEE Aerospace Conference Proceedings 2017*, IEEE, Big Sky, MT, 2017.

[11]Wilder, M. C., Bogdanoff, D. W., and Cornelison, C. J., "Hypersonic Testing Capabilities at the NASA Ames Ballistic Ranges," *53rd AIAA Aerospace Sciences Meeting*, American Institute of Aeronautics and Astronautics, Kissimme, FL, January 2015.

[12]Bogdanoff, D. W. and Wilder, M. C., "Upgrades and Modifications of the NASA Ames HFFAF Ballistic Range," *To be presented at the 68th Meeting of the Aeroballistic Range Association*, Monterey, CA, 2017.

[13]Yates, L. and Chapman, G., "Aerodynamic ballistic range analysis using generalized math models," *21st Atmospheric Flight Mechanics Conference*, American Institute of Aeronautics and Astronautics, San Diego, CA, July 1996.

[14]Canning, T. N., Seiff, A., and James, C. S., *Ballistic-Range Technology*, AGARDograph No. 138, 1970, pp. 207-210.

[15]Bogdanoff and W., D., "Design Guide for Aerodynamics Testing of Earth and Planetary Entry Vehicles in a Ballistic Range," 2017.

[16]Subbareddy, P. K. and Candler, G. V., "A fully discrete, kinetic energy consistent finite-volume scheme for compressible flows," *Journal of Computational Physics*, Vol. 228, No. 5, 2009, pp. 1347–1364.

[17]Spalart, P. and Allmaras, S., "A one-equation turbulence model for aerodynamic flows," *30th Aerospace Sciences Meeting and Exhibit*, American Institute of Aeronautics and Astronautics, Reno, NV, January 1992.

[18]Wright, M. J., Candler, G. V., and Bose, D., "Data-Parallel Line Relaxation Method for the Navier-Stokes Equations," *AIAA Journal*, Vol. 36, No. 9, September 1998, pp. 1603–1609.

[19]Pointwise, I., "Y-Plus Calculator - Compute Wall Spacing For CFD," http://www.pointwise.com/yplus/, Retrieved: July 2016.

[20]Soumya Dutta, "Program to Optimize Simulated Trajectories II (POST2)," Ver. 4.0D, NASA Langley Research Center, Hampton, VA, November 2016.